ORIGINAL PAPER

Analyses of optical images and radar data reveal structural features and predict groundwater accumulations in the central Eastern Desert of Egypt

Mohamed Abdelkareem · Farouk El-Baz

Abstract The North African Sahara is currently dominated by arid to hyperarid climate. In the central part of the Eastern Desert of Egypt, Wadi Matula is a dry stream course much like those in the rest of the Sahara. It covers an area of about 7,500 km^2. Radarsat-1 images, Shuttle Radar Topography Mission (SRTM), and Advanced Land Observing Satellite (ALOS)/Phased Array type L-band Synthetic Aperture Radar (PALSAR) data revealed paleodrainage systems and fault/fracture zones. Its trends display cross-cutting relationships. Interrupted surface runoff connections are inferred from block movements, tectonic capture processes, diverted valleys, and paleodrainage. The movements of the blocks led to newly formed drainage and caused disturbances in drainage orientations, topography, fractures, and stream density. Paleodrainage and the more recent drainage lines are superposed on weakness zones of major fractures and faults. These zones facilitated the hydrologic processes that caused erosion and downcutting. The intersection points of paleochannel courses, fracture/fault systems, and active streams must have increased the possibilities of groundwater accumulations. Accordingly, several exploration wells are suggested, which they represent the best abstraction sites of groundwater potentials. These predicted sites are consistent with the high potential zone of the groundwater prospect map. Thick fluvial deposits support that past pluvial events recharged the underlying aquifers. It is concluded that locations of paleodrainage, fractures/faults, and stream intersections are the best sites for groundwater resources; thus, radar images are powerful tools for mapping multi-temporal near-surface features in arid regions.

Keywords Radar data · GIS · Tectonics · Groundwater

M. Abdelkareem (✉)
Geology Department, South Valley University, Qena 83523, Egypt
e-mail: mohamed.abdelkareem@sci.svu.edu.eg

M. Abdelkareem
e-mail: mismail@bu.edu

F. El-Baz
Center for Remote Sensing, Boston University, 725 Commonwealth Ave., Boston, MA, USA

Introduction

Remote sensing data have provided information on the Earth from space, allowing the collection of several digital images that have helped in the study of our planet. This tool can be used for detecting paleomorphologies of landscapes at different spatial resolution (e.g., Mertes 2002; Hayakawa et al. 2010). Technological advances have allowed imaging in progressively higher spatial and temporal resolution. This also allowed penetrating clouds and contributing on the estimation of rainfall and cloud volume.

The optical sensors measure electromagnetic (EM) radiation that is reflected by the Earth's surface. The chemical composition of the object is a function of the reflected radiation in the visible region. However, the interaction between electromagnetic radiation and an object in the microwave region (radar waves) generates information related to the geometry and surface roughness of that object and what are known as "dielectric properties" of the object, which generally are closely correlated with its moisture content (e.g., Paul and Koch 2011).

Roth and Elachi (1975) illustrated that radar waves have the ability to produce images of the subsurface, particularly in arid regions to the depth of several meters (Paillou et al. 2009). Thus, such views from space are extremely valuable to regional geological reconnaissance, particularly in the study of surface and near-surface features in arid areas. In 1981, National Aeronautics and Space Administration (NASA)

acquired such images using the Shuttle Imaging Radar-A (SIR-A) that showed paleochannels beneath sand sheets in the Sahara at Bir Safsaf region, in southern Egypt (McCauley et al. 1982). Later, SIR-C ($\lambda = 5.8$ cm), Shuttle Radar Topography Mission (SRTM), and Radarsat-1 ($\lambda = 5.6$ cm) as well are used C-band. The depth of the used C-band of the subsurface penetration for imaging is about 0.5 m (Schaber et al. 1997). This penetration of the electromagnetic energy depends on the terrain properties, i.e., nature of the rocks and moisture content (e.g., Robinson et al. 2000).

The radar data were employed widely in mapping surface and near-surface drainages that were difficult to verify by either optical images or field observations. Thus, they proved to be excellent tools for mapping ancient fluvial features in the desert, which were covered by sand sheets and dunes prior to any field measurements (El-Baz 1998). Radarsat-1 images using C-band can be used in mapping morphologically defined structures and features (Abdelsalam et al. 2000; Gani and Abdelsalam 2006; Thurmond et al. 2006).

Several studies (e.g., McCauley et al. 1982, 1986; Schaber et al. 1997; El-Baz 1998; Robinson et al. 1999, 2000; El-Baz et al. 2001) showed past hydrological processes with indirect indications of the possibilities of the groundwater resources. Because the revealed paleochannels must have hosted vast volumes of runoff during past tropical conditions, vast groundwater amount must have been accumulated (El-Ramly 1980; El-Baz 1998). Water would have seeped into the substrata through fluvial deposits. Therefore, areas that received large fluvial accumulation in this part of the Sahara during the tropical conditions would host vast groundwater resources (El-Baz 1998).

The objectives of the present study are to process and analyze radar and optical images that cover the study area and combine them in a GIS to understand the past hydrological processes. The study also aims to investigate and predict the best locations of groundwater potentials based on multiple criteria.

Study area

Wadi Matula covers a large tract that extends from the Red Sea Mountains to the Nile Valley between longitudes 32° 48′ 00″ E and 34° 30′ 00″ E and latitudes 25° 46′ 00″ N and 26° 04′ 00″ E (Fig. 1). It is located east of the middle section of the Nile Valley in the Eastern Desert of Egypt. It covers approximately 7,500 km². Its current tributaries drain the Red Sea highlands during sporadic rainfall events and flow downhill where they join the Nile River at Qift City. It is a large and wide valley that extends westward about 130 km from its eastern end. It has an E-W trend and gently dips to the west until it joins the Nile River at Qift City. Its major tributaries include Wadi El-Hammamat, Wadi Zaidun, Wadi El-Mishash,

and Wadi El-Muweih. Wadi El-Hammamat was named after the Bath Springs "El-Hammamat" of Cleopatra, Queen of Egypt, since 2,000 years ago. There are numerous ancient well remnants of the Pharaonic and Roman periods along the ancient Qift-Qusier route. The area is promising for agriculture and thus the need for groundwater exploration.

The area includes several ancient wells (Birs) including Hammam Cleopatra, Bir Lakita, and Bir Fawakhier. The watershed of the present study is selected because it converges to join the Nile Valley between Qift and Qena cities. Furthermore, the geomorphic characteristics, tectonic disturbances, abundant cross-cutting relationships, closeness to the Red Sea highlands, and the presence of paleodrainage features add to groundwater potentials. Moreover, the valleys are close to large urban and industrial areas that require new water resources.

In physiographic terms, the present study (Fig. 1b) can be divided into three geomorphic units: the Red Sea highlands (basement rocks), plateau of Upper Cretaceous/Lower Tertiary sedimentary sequence and wadi floodplains. Based on the geological map by Conoco (1987), the Red Sea highlands are dominated by Precambrian basement rocks, unconformably overlain by a variety of Phanerozoic rocks. The massive plateau is made up of sedimentary sequences that unconformably lie on the basement rocks. These sedimentary rocks of Cretaceous/Tertiary age are topped with a massive limestone layer. The wadi filling is a low-lying area along the basement rocks to the east and the plateau to the west. This plain is occupied by thick deposits of sand and gravel.

Faults and fractures are the prominent structural features in the area. These have several trends including NW-SE (Gulf of Suez or Red Sea trend) NNW-SSE, WNW-ESE, and ENE-WSW (Said 1981; Schurman 1956; Abdel Razik and Razvaliaev 1972; Awad 1981) much like Eastern Desert trends. The area under investigation is highly fractured and still subject to tectonic reactivation as a result of the Red Sea tectonics.

From the hydrologic point of view, the area is located in an arid-to-hyperarid region that receives less than 100 mm of rains on average per year (Gheith and Sultan 2002; Sultan et al. 2008). Given the modern hydrograph by Tropical Rainfall Measuring Mission (TRMM) data, the mean daily rainfall data in a period of 1998 to 2012 ranges from 0.0045 to 0.03 mm/day (Fig. 2a). This reveals extremely low rainfall. The average rainfall increases northward and eastward, toward the Red Sea coast. The surface hydrology of the area mainly comprises surface runoff and drainage during rainfall seasons and flash floods along the high altitude of the Red Sea Hills. Therefore, groundwater is the only permanent water resource in the area with varying depths as subbasins. Shallow groundwater aquifers in wells mostly occur within the alluvial deposits, which vary from clay to gravel and boulders. The main recharge is from the uneven local rainfall

Fig. 1 The Egypt's Nile region. **a** The Nile River and Nile Delta marked by the *blue line*; the watershed of the study area is marked by the *green line*; **b** geological map of the present study (after Conoco 1987). Qift-Qusier Road (marked by *solid black*) that links the Nile Valley to the Red Sea, across the study area
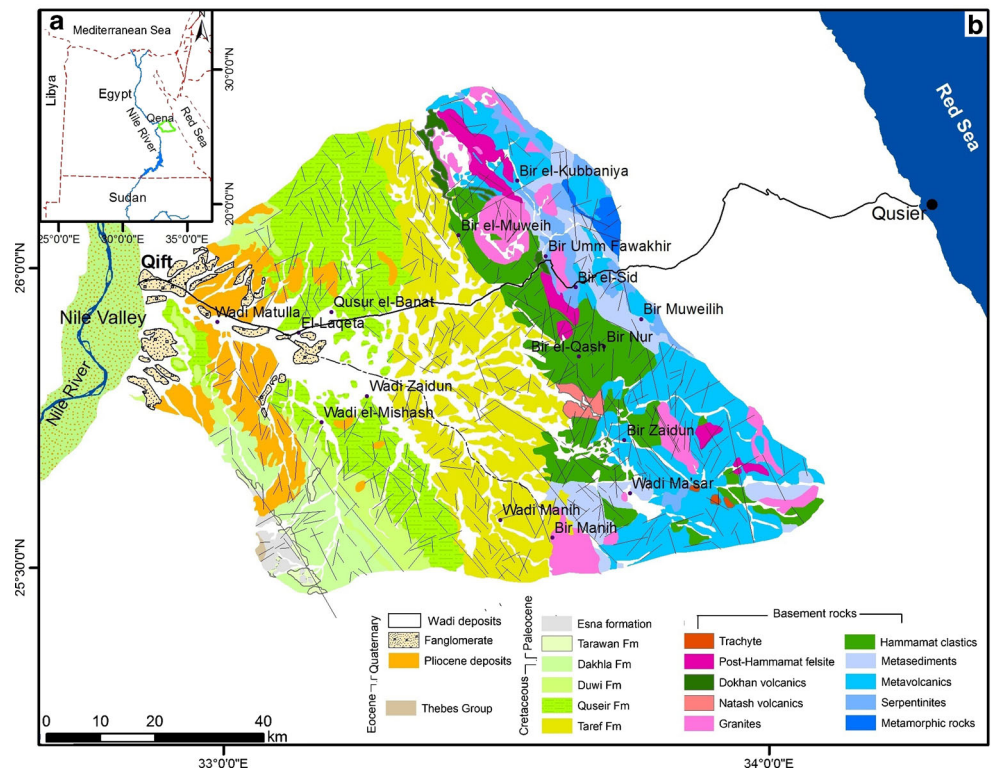
and flash floods due to short-period heavy storms that are driven by high altitude of the Red Sea Hills.

Material and methods

Integrations of Synthetic Aperture Radar (SAR) from Radarsat-1 and SRTM data were used in the present study. False color combination 7,4,2 (RGB) of Landsat Enhanced Thematic Mapper Plus (ETM+, spatial resolution 30 m) and automatically extracted drainage networks were used to validate the active (ephemeral) streams. Rainfall precipitation date (mm/day) data from TRMM were used. Geological maps (Conoco 1987) and field observations (including well locations and fluvial deposits) are used to complement satellite image analysis and interpretations.

Radar data

Radarsat-1

SAR data from Canadian Radarsat-1 satellite using a single frequency =5.6-cm horizontally polarized C-band with 12.5-m pixel spacing were used here because the C-band radar signals penetrate dry sand cover. The fine-grained deposits would appear dark as a result of specular reflection of the radar wave away from the receiving antenna; whereas coarse-grained deposits or rough surfaces would appear light because of diffuse reflection (Jensen 2000).

The image georeferencing and transformation were carried out using the ENVI 4.8 software. The image transformation process was performed using ground control points (GCPs) and applying the cubic resampling method. The Enhanced Lee filter (Laplacian edge enhancement) was applied with a 3 size window to reduce the effect of speckle and improve the visual interpretation. The data were enhanced by linear scaling from 16 to 8 bits based on image histograms followed by a Gaussian stretch. Digitizing of the paleochannels using ArcGIS 9.3.1 software packages was used to detect the paleochannel pathways and their relation with the present landscape. These channels could be used to identify the groundwater potentials and suggest locations of abstraction wells.

SRTM

The SRTM is a joint project of NASA and the National Geospatial-Intelligence Agency (NGA). Its data are of an ~90-m horizontal resolution and are available from the Global Land Cover Facility (http:glcf.umiacs.umd.edu/index.shtml). The SRTM digital elevation model (DEM) was used in extracting of stream networks (Fig. 2b). This was done by employing surface flow routing based on the 8D flow direction algorithm of Jenson and Domingue (1988). This was done using a hydrology module of spatial analyst in
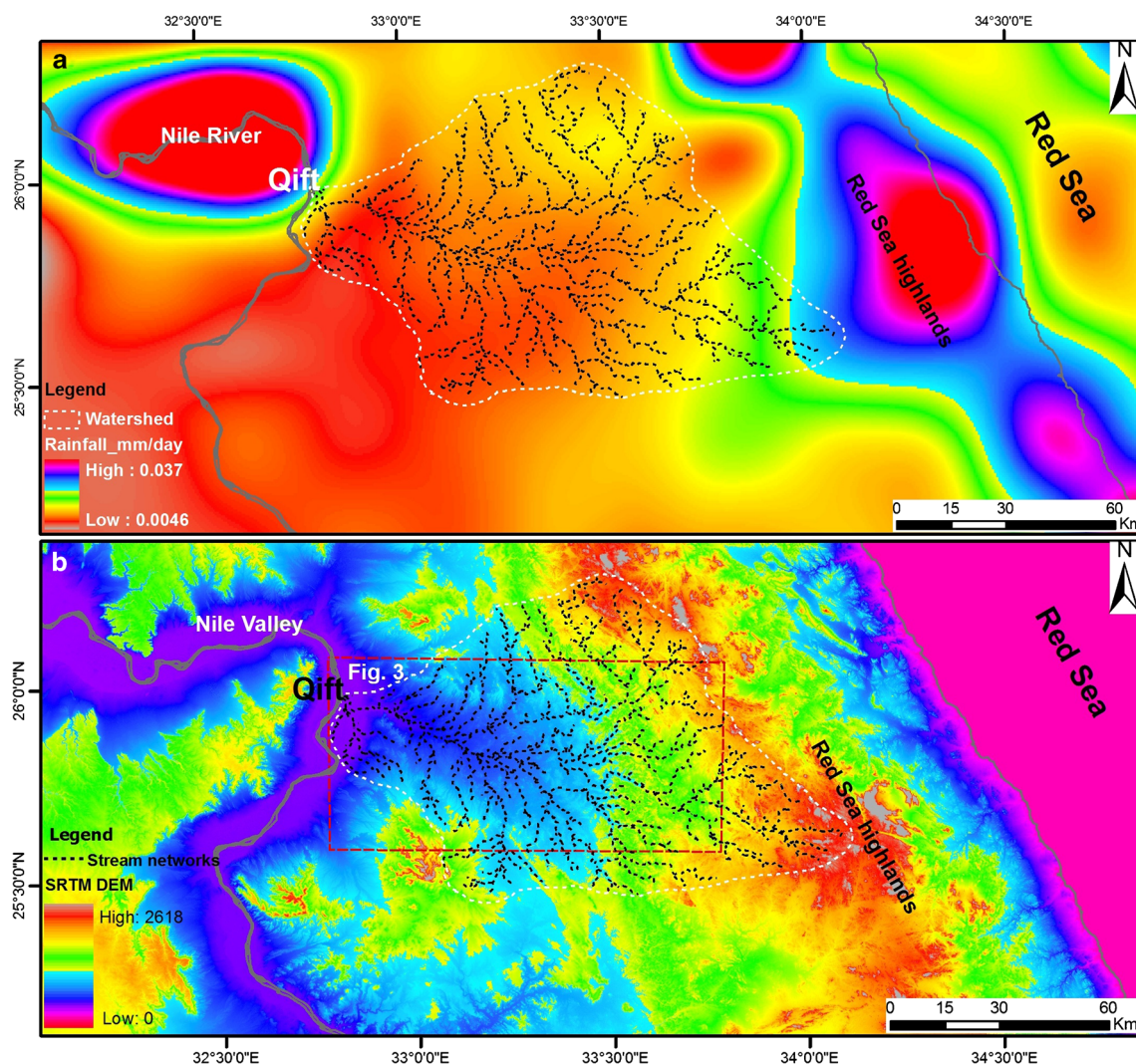
Fig. 2 Radar data. **a** Tropical Rainfall Measuring Mission (TRMM) data with the extracted drainage channels marked by *dark dashed lines*; **b** digital elevation model (DEM) based on the Shuttle Radar Topography Mission (SRTM, showing the elevation in the study area) watershed marked by the *white dashed line*

subsequent steps including filling sinks, flow direction, flow accumulation, and stream delineation steps to extract the stream network (e.g., El Basstawesy et al. 2010; Abdelkareem et al. 2012b; Abdalla 2012).

ALOS/PALSAR

The Advanced Land Observing Satellite (ALOS)/Phased Array type L-band Synthetic Aperture Radar (PALSAR) is an active microwave sensor using L-band frequency. It is a joint project between JAXA and the Japan Resources Observation System Organization (JAROS). The ALOS/PALSAR L-band (1.27 GHz, 24 cm) scene (product level 1.5) was acquired on January 26, 2008 with an incident angle of 34.3°. This scene was used in this work to view the near-surface structures in the present study area in comparison

with the Radarsat-1 data. The view was enhanced using Enhanced Lee filter (Lopes et al. 1990), with applying a 3 size window to reduce the effect of speckle and improve the visual interpretation.

TRMM data

The TRMM was successfully launched on 27 November 1997 from the Tanegashima Space Center in Japan (Kummerow et al. 1998). In the present study, the TRMM data were collected on Wadi Matula region from 1998 to 2012 to understand the main catchments area; these data are available on the website: "http://trmm.gsfc.nasa.gov/." These accessed precipitation data were interpolated using the Kriging method of the ArcGIS Spatial Analyst tool to map the high anomalies of rainfall.

Optical images

Landsat ETM+

Landsat 7 data that was successfully launched in April 1999 are accessed from the Global Land Cover Facility (http:glcf.umiacs.umd.edu/index.shtml) and were used for image processing and data fusion. Six ETM+ bands 1–5 and 7 (30-m resolution) were used. The recent active (ephemeral) streams were digitized using the bright signature of the 7,4,2 (RGB) false color band combination as compared to the surroundings.

ASTER images

Advanced Spaceborne Thermal Emission and Reflection (ASTER) is an instrument sensor system aboard the satellite Terra launched on December 18, 1999. Aster Level 1b (L1b) processed data are available in the USGS website (http://glovis.usgs.gov/). One scene covering the downstream area of the present study was acquired and processed using ENVI v. 4.8.

Fusion of optical-radar images

The image fusion is a process that integrates images from different data sources to reveal more information than can be separately derived from any of them alone (e.g., Pohl and van Genderen 1998; Ricchetti 2001; Amarsaikhan et al. 2009; Abdelkareem et al. 2012b). Data fusion was done by applying a hue, saturation, and value (HSV) sharpening transformation of Envi 4.8. Image sharpening is commonly used to sharpen a low spatial resolution multiband image by a high spatial resolution image. However, the integration of band combination 7,4,2 (RGB) Landsat image and Radarsat-1 is used here to produce hybrid images that combine information of spectral properties (from the ETM+ image) and surface roughness (Radarsat-1 image) to improve visual interpretation of morphotectonic features and drainage systems.

Results and discussion

Based on the results of radar image analysis and interpretation, the ancient Wadi Matula probably was subjected to strong hydrological processes during pluvial events in the past. This is revealed from the denudation and the sizable fluvial deposits in the region. The present main course of Wadi Matula has high runoff westward as revealed from the automatically extracted drainage channel networks and elevation values derived from the DEM (Fig. 2b).

Radarsat-1, ALOS/PALSAR, and fused optical/radar images (Fig. 3) probe the sand cover and show near-surface views that allowed detection of paleodrainages and a probable fault/fracture zones that are barely visible in the enhanced optical ETM+ images (Fig. 3a). The filling deposits appear dark in Radarsat-1 images versus the intermediate to bright outcrops of surface bedrocks reflecting textural information based on surface roughness (e.g., Zebker et al. 1996; Abdelsalam et al. 2000). The dark signatures are probably due to the porous fine-grained fluvial deposits of sand which facilitate penetration of electromagnetic radar wave. Thus, the more penetrating electromagnetic waves were reflected later than the less penetrated one, showing differences in the reflected wavelengths (retardation) detected by the sensor.

The dimension and geometry of the investigated features were clearly shown in Radarsat-1 images (Fig. 3b). The streams at the upstream area appear as narrow incised channels that become broader and converge toward the downstream. The fused Radarsat-1/ETM+ image (Fig. 3c) offered better observations than using individual images. This image distinctly enhanced views of incised channels and fault/fracture line traces by integrating the surface roughness of Radarsat-1 and the spectral signatures of ETM+ image. This is witnessed in the straightness and the sharpness of the radar illumination and shadow stripes that define the border faults/fractures, scarps, and ridges. A subset of available ALOS/PALSAR (Fig. 3e) shows even more incised channels resulting from the electromagnetic L-band than the C-band of Radarsat-1 and ETM+ (Fig. 3a, d). The fused subset of both ALOS/PALSAR and ETM+ shows finer resolution and more penetration in comparison to both Radarsat-1 and the optical image, respectively (Fig. 3d–f). This is because the L-band of PALSAR data provides even deeper penetration than the C-band and could define the hidden fault lines and structural geometry as well (e.g., Gaber et al. 2011).

The data also provide evidences for tectonic piracy resulting of active tectonic movements. The incisions of E-W lineaments crossed and captured the N-S and NW trends (Fig. 3d), providing further evidence for an episode of tectonic reactivation. The clear observations of near-surface views allowed tracing cross-cutting relationships of fault/fracture lines in NW-SE and E-W directions (Fig. 4). The digitized paleochannels emphasized the tectonic capture processes. To validate the stream capture processes and cross-cutting relationships, the active stream networks of the recent flash flood, the digitized paleochannels, and the automatically extracted stream networks are superposed. The active (ephemeral) streams have spectrally bright appearance compared to the brownish color of the surroundings in the false 7,4,2 (RGB) band combination, respectively, of ETM+ images (see Fig. 5a, b). Rainfall precipitation over the Red Sea highlands channeled these streams during short heavy storms.

Most of the active streams through Wadi Matula often show concordant relationships with the automatically extracted and the digitized paleochannels. The discordant relations
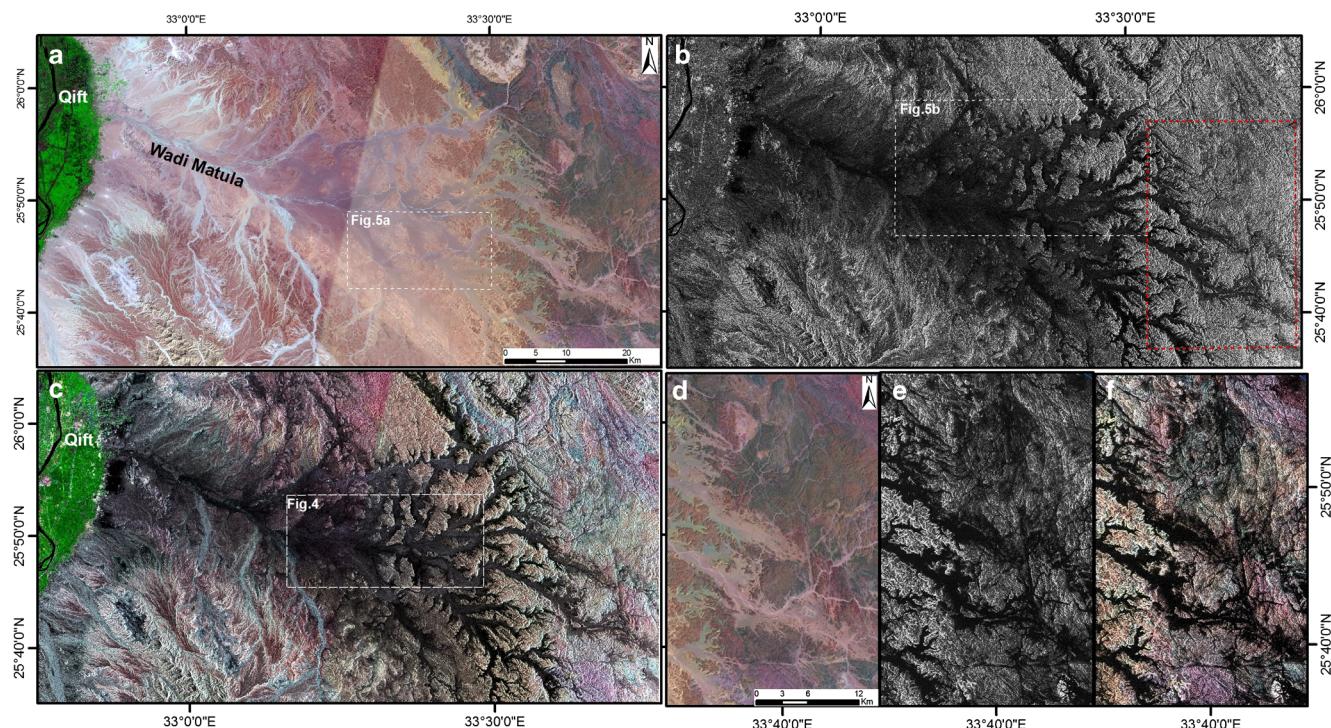
Fig. 3 Optical and radar data. **a** False color band combination 7,4,2 (RGB) Landsat ETM+ image of the present study area; **b** Radarsat-1 image covering the same area showing drainages that are marked by the *darker signature* compared to the surroundings; the *red dashed box* shows areas in **d**, **e**, **f**; **c** fused Radarsat-1 and ETM+ hydride image enhance the view of faults by sharpening the morphological define structure; **d**, **e**, **f** subset of ETM+, ALOS/PALSAR, and fused ALOS/PALSAR and ETM+ images, respectively showing parts of the study area. The ALOS/PALSAR image using L-band reveals more penetration and finer resolution than ETM+ and Radarsat-1, respectively
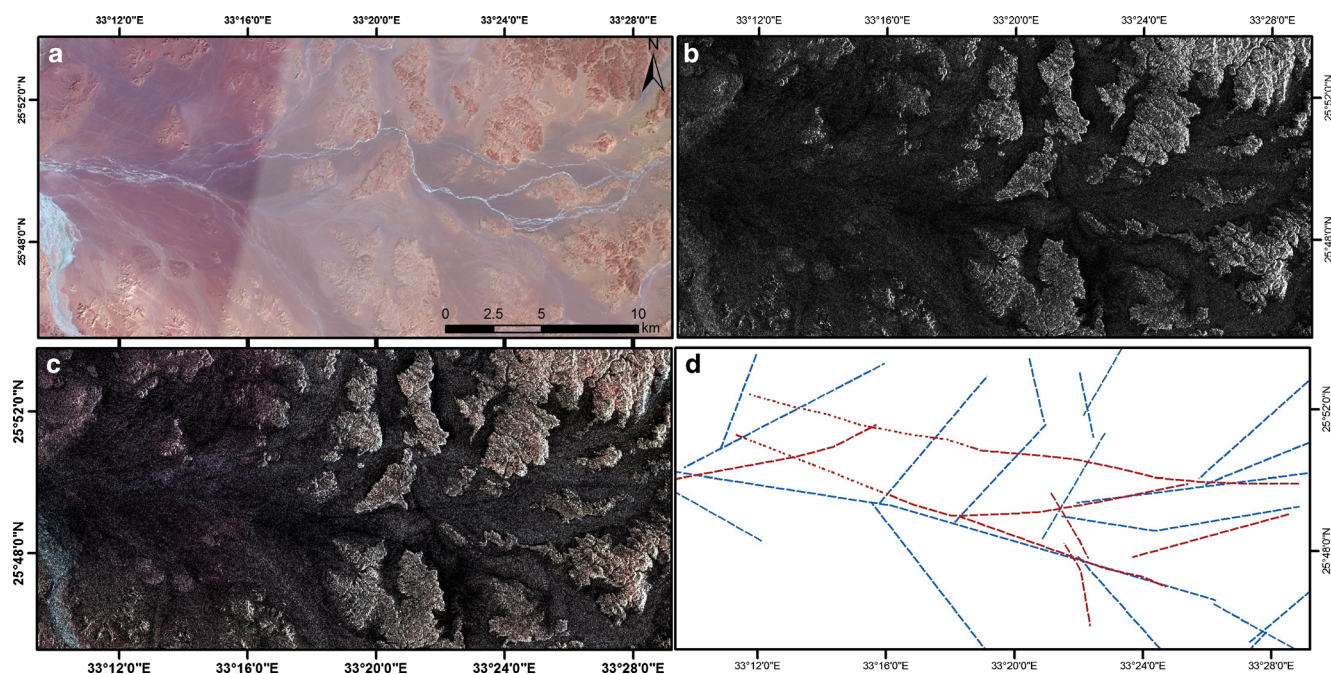
Fig. 4 Subset of Landsat ETM+, Radarsat-1, and fused Landsat ETM+/ Radarsat-1 image as shown in Fig. 3; **a** false color band combination 7,4,2 (RGB) ETM+ image covering a part of Wadi El-Hammamat shows bright signature of the active streams, with no lineaments and structural features; **b** Radarsat-1 image covering the same area displays the near-surface view and appearance of lineament features; **c** fused Radarsat-1 and ETM+ images enhancing the near-surface and lineament views in comparison to optical and radar image alone; **d** extracted lineaments mapped by Radarsat-1 image and fused Radarsat-1 and ETM+ images; a probable near-surface lineaments are marked by *dashed red lines* and *dotted red lines* likely matched with desert tracks
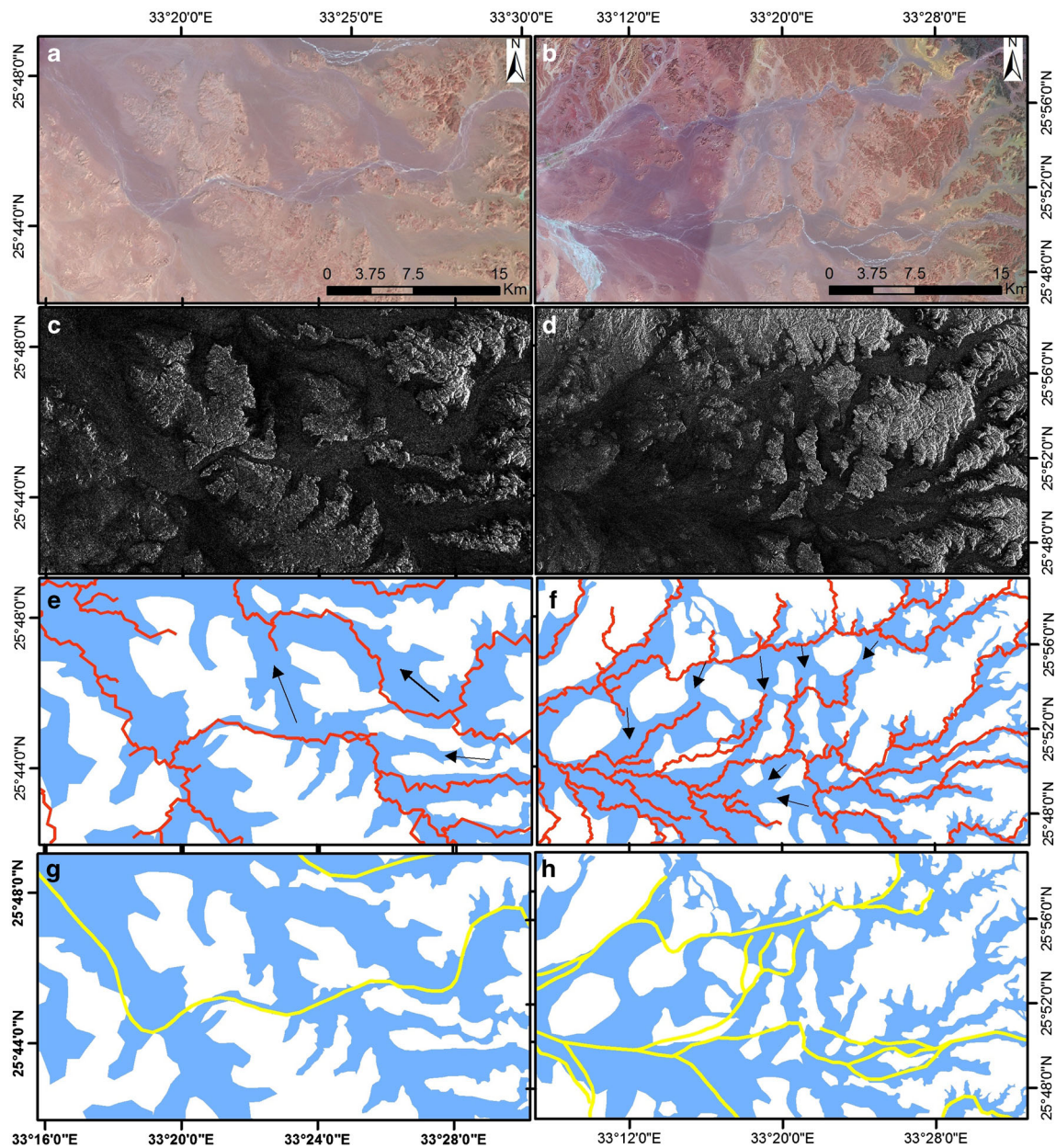
Fig. 5 Stream capture processes. **a**, **b** False color band combination 7,4,2 (RGB) of Landsat image covering part of Wadi El-Hammamat showing bright signature of the active streams; **c**, **d** Radarsat-1 image showing incised channels with near-surface lineaments; **e**, **f** digitized paleochannels with automatically extracted stream networks marked by *red lines*; the *black arrows* point to the direction of old pathways; **g**, **h** digitized paleochannels with active streams of the most recent flow that indicate the stream capture direction, while digitized areas in *blue* show stream flow direction prior to the capture processes

are obvious in most active tectonic areas. The discordant active streams are directed to flow through the recent faults of E-W trend. The acute and right angle intersections between the NW trend and E-W trend lines have demonstrated results of tectonic capture processes. As shown in Fig. 5, the present flow directions recorded by the automatically extracted drainage networks coincide with the red line (recent pathways), instead of following the digitized blue areas of the old pathways. However, active streams (marked by yellow) extracted from ETM+ reveal that the most recent runoff is roughly

coincident with the automatically extracted drainage networks (Fig. 5g, h). This is because the E-W active tectonics of the Red Sea that continue since Neogene probably captured the earlier N-S stream flows.

Tectonic movements of the Red Sea caused disturbances in the drainage orientations as inferred from the presence of relics of the paleochannels and tectonic capture processes. Therefore, changes in the hydrological processes, i.e., runoff direction, and recharge and discharge processes are common. The paleodrainages that have a NNW trend appear mature,

with some diversion, and show cross-cutting relationships with the E-W fault lines. This is indicated by the right angle intersections between both NNW and E-W trend lines. As a result, the stream capture processes are most likely common among these drainage lines. Most of these channel courses were probably connected northward with the earlier Qena system (Abdelkareem 2012).

The digitized paleodrainage systems reveal clear remnants of the ancient pathways in Fig. 6. These paleodrainage channels ran east of the sedimentary hills and were forced to follow the westward trends as evidenced by the diverted flow direction of drainages and right angle intersections. The westward tectonic piracy of the aligned N-S channels that ran parallel to the strike of the unconformable basement/sedimentary contact

revealed evidence that the wadi probably drained northward upon connection with the ancient Qena River (Abdelkareem 2012; Abdelkareem et al. 2012a). This connection was before the breaking apart of the massive plateau in E-W direction since the gravel did not reach the present channel of Wadi Matula before the Middle Pleistocene Epoch (Sandford 1929).

Capture processes based on the interpretation of integrated data, evidences and observations of clear near-surface views including faults/fractures, and paleodrainage courses were detected. Accordingly, the presence of cross-cut relationships and reorientation demonstrate tectonic reactivations through times. These are evidenced by the presence of remnants of paleodrainage lines and low topographic areas that extend from Wadi Qena to Wadi Matula (Fig. 6). Abdelkareem

Fig. 6 Illustrations of Wadi Matula, digitized paleochannels using Radarsat-1 image, and movement of the blocks marked by *white polygons*: **a** boundary of watershed overlain on ETM+ image as a *yellow line*, with boundaries of structurally coherent blocks in *dotted white lines*; Qena-Safaga Shear Zone marked by the *solid white line*; **b** Radarsat-1 image showing a dark signal of the fine deposits along the main stream; **c** digitized channels derived from Radarsat-1 mosaic; **d** SRTM data showing a wide downstream area with stream networks
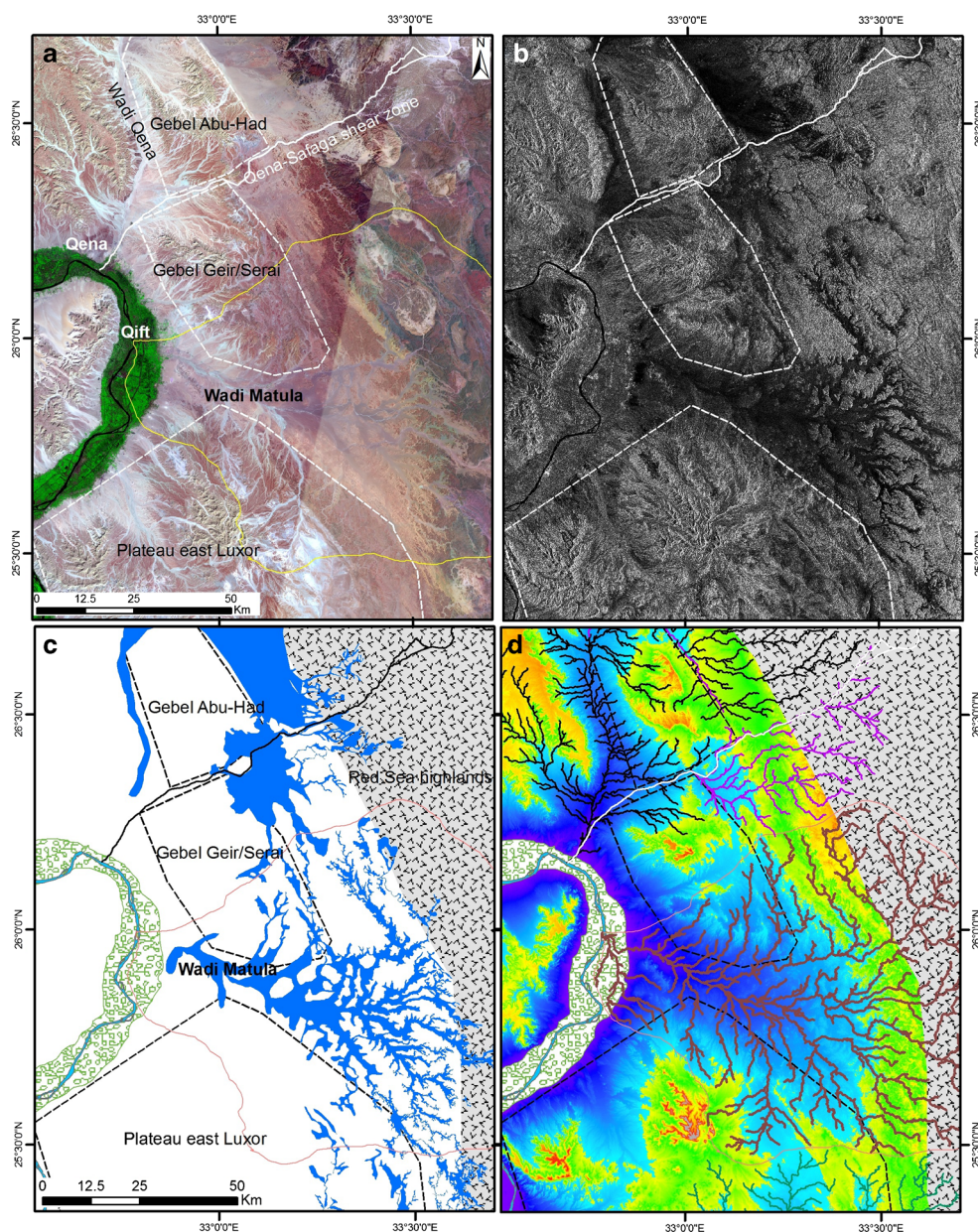
(2012) clearly traced the north-trending river course of Wadi Qena that connected Wadi Matula and Wadi Batur. Moreover, the area between Qena and Qift cities was subjected to tectonic disturbances that caused diversion of channel pathways.

Groundwater implications

The interpretation of radar images shows fault and fracture systems in the present study. These tectonic lineaments converge and join the mainstream, allowing the prediction of best locations for wells and springs (e.g., Babiker and Gudmundsson 2004). The area under investigation is highly fractured (Fig. 7a) and was subjected to lateral and vertical movements (e.g., faults and fractures). These movements impacted the drainage courses and probably the groundwater aquifers in the region. Several studies employed tectonic element intersections on groundwater discharge and recharge processes (e.g., Babiker and Gudmundsson 2004; Sultan et al. 2008).

The tectonic capture process in the present study reveals active fault and fracture systems that probably act as a medium for the surface water infiltration to recharge the underlying aquifers, because they could have acted as storage zones, collectors, or transmitters for groundwater. The fracture and fault systems can have controlled groundwater fluxes and helped in predicting the most important sites for groundwater wells, because fractures cause secondary porosity and

Fig. 7 a Lineaments mapped in the study area; *black lines* represent lineaments from the geological map (Conoco, 19887) and stream networks. The extracted lineaments from Radarsat-1 images are marked by *blue lines*, and the probable near-surface faults are marked in *red lines*. The rose diagram shows the distribution of tectonic trends; b digitized paleochannels from Radarsat-1 image with the extracted stream channels, active stream flow pathways (*yellow lines*), and the probable near-surface faults (*red lines*). The present wells are marked in *green points*, and the suggested wells are marked in *red solid circles*
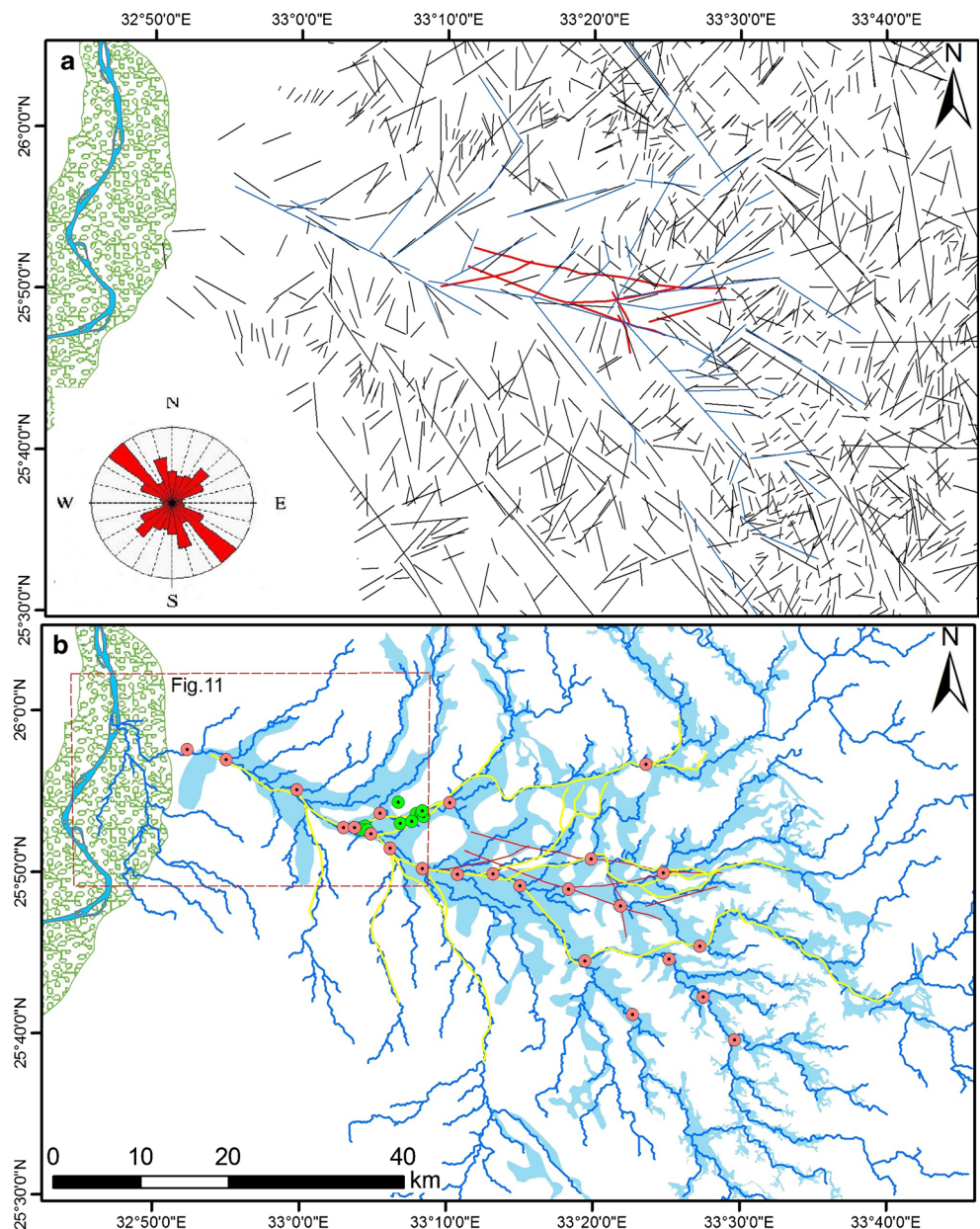
**Fig. 8** Simplified flow chart showing the integrated layers in GIS
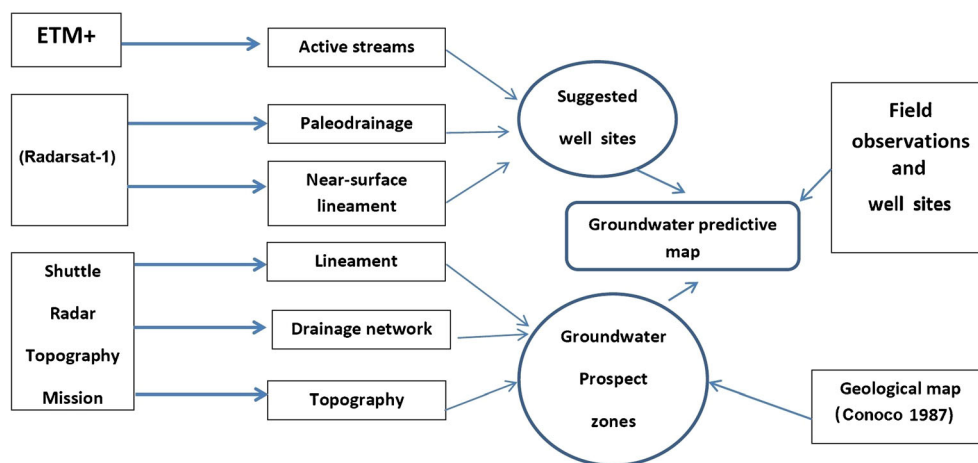
hydraulic conductivity that enhance well yields (Das et al. 1997). They also facilitate the recharge and discharge processes, particularly at the intersections between active channels, faults, and paleodrainage. Thus, the intersection points of fault systems, active streams, and paleodrainage courses probably increase the possibilities of groundwater potentials (Fig. 7b). The subsurface structural elements also controlled the storage and movements of groundwater flows. Accordingly, several exploration wells were suggested within the study area, based

on the intersection points, which may represent the best sites of borehole groundwater abstraction (Fig. 7b).

In addition to the tectonic elements, understanding the locations of paleodrainages is extremely important in predicting the best locations for groundwater potential, because they must have received surface water in the past pluvial conditions (see Fig. 7b, digitized in blue color). This is because the received fluvial sediments have high porosity and hydraulic activity; these are much suitable for storing the

Fig. 9 Thematic map layers as derived from satellite images and extracted lineaments. **a** Stream density map; **b** lineament density map; **c** digital elevation model (DEM) classified map depending on water infiltration; **d** integrated map of topography, stream, and lineament density showing variations of zones for groundwater accumulation superimposed by the present wells (marked by *blue solid circles*) and the suggested wells in *green points*
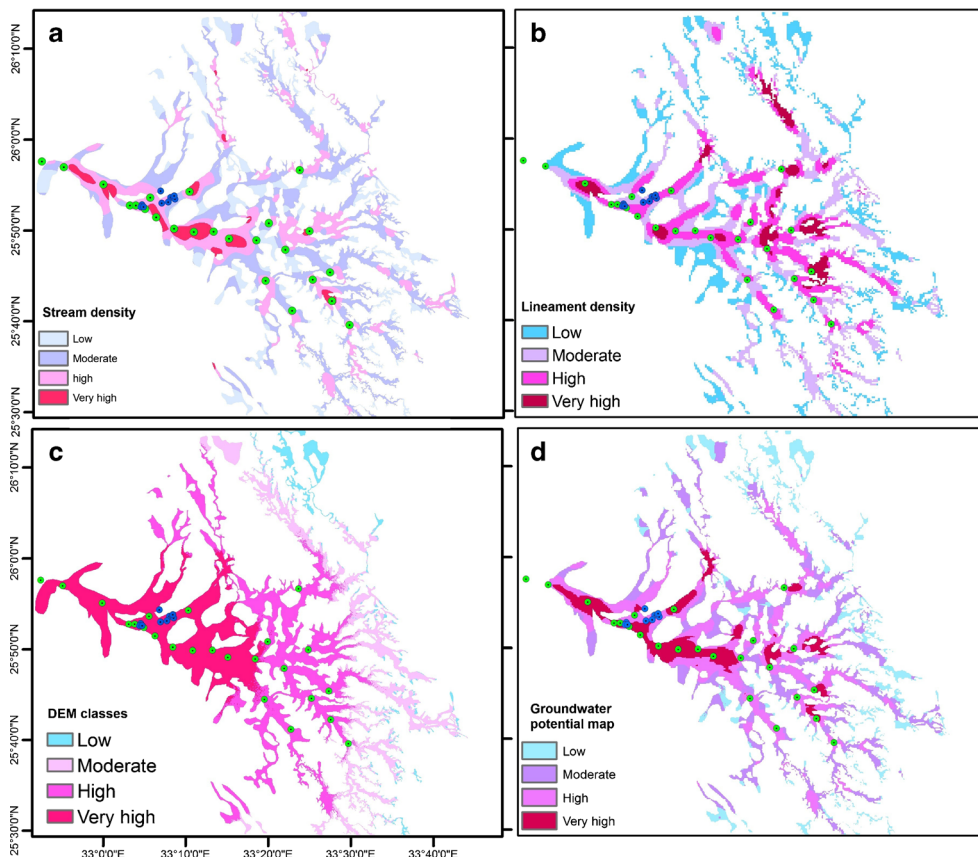
infiltrated surface water (El-Baz 1998). Thus, the digitized paleochannels may represent best area for groundwater accumulation for use in human activities. However, the movements and infiltrations of runoff are influenced by other factors, e.g., fracture, topography, paleodrainage courses, and drainage networks of the present landscape. These factors are integrated using ArcGIS software packages as shown in Fig. 8, to predict the best locations for groundwater accumulation (Fig. 9). For example, high stream density, high lineament density, and the lowest topography (Fig. 9a–c, respectively) could be considered as probable prime locations for subsurface water infiltration and accumulation (e.g., Abdelkareem et al. 2012b; Abdalla 2012), whereas low drainage and lineament density and high topography areas could be assigned lower groundwater accumulation. The latter areas represent the best areas for holding groundwater. These criteria

are integrated in layers using ArcGIS to get the best zones for groundwater potentials, considering the digitized paleochannels as a mask for the investigated area. Well locations validated the best zones for groundwater accumulation. This approach is economical, valuable, and applicable throughout arid regions, such as the eastern Sahara, where the evaluation of water availability is vital to the increase of food production to alleviate population pressures and other activities.

Field observations revealed past hydrodynamic activity that facilitated the downcut and erosion processes as seen in remnant cliffs (Fig. 11a) and ample fluvial deposits. Sites of intersections between paleodrainage courses, active streams, and extracted stream networks have been investigated during field visits. The discharge flows of well numbers 6, 8, and 9 along (Figs. 10b and 11b–e) Wadi El-Hammamat and Zaidun

Fig. 10 a Aster image covering the downstream area with present water wells (*green points*) and the suggested wells as *red points*; b digitized paleochannels marked by *cyan color* superimposed by stream networks (*blue lines*), active streams (*yellow lines*), and radar faults; present well (marked by *green solid circles*) and suggested wells in *red solid circles*
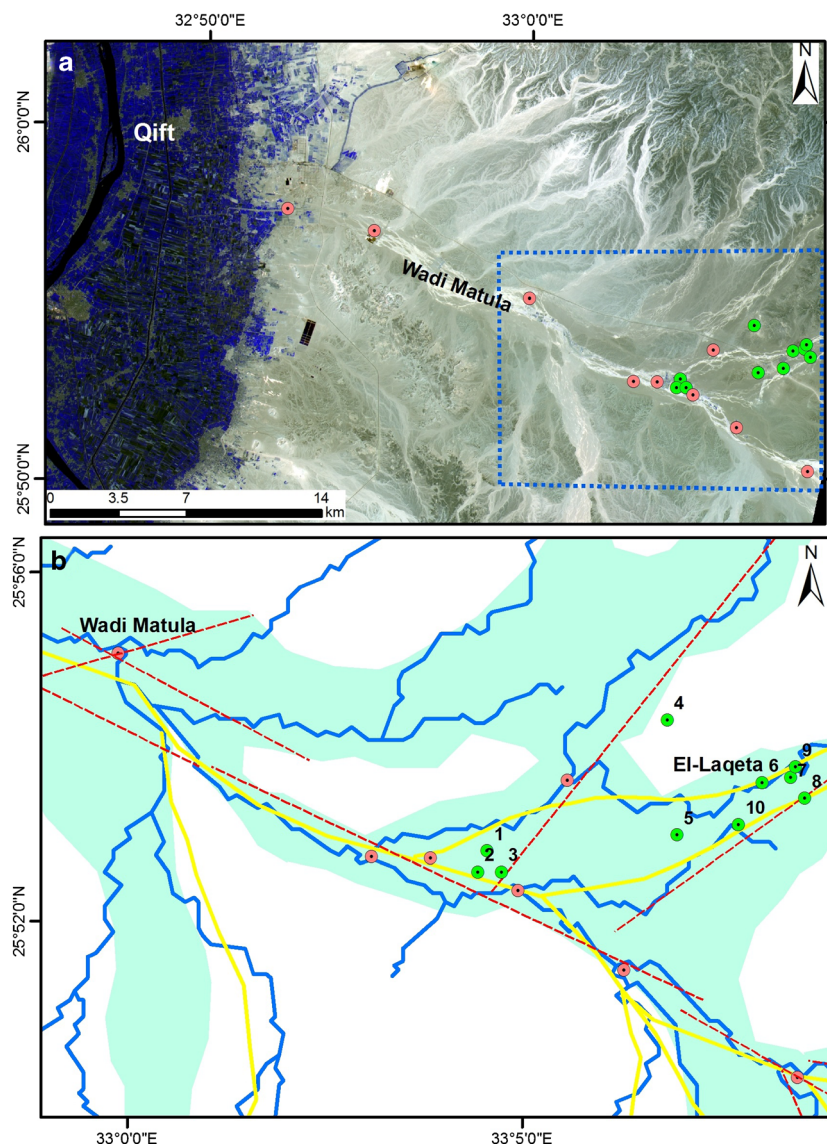
Fig. 11 Field photographs of the present study area. **a** Cliffs of the Nubian Sandstone along Wadi Hammamat reveal strong hydrological processes in the past; **b** ancient Roman well number 9 and **c**, **d** well numbers 6 and 8, respectively; a highly productive well within Nubian Aquifer; **e** excavated water trench; **f** a highly productive well-like spring (number 7), this photo was taken by Abdalla (2012)

are probably facilitated by deep-seated aquifers of fossil water, where tectonic elements increased the hydraulic activities (Gudmundsson 2001; Babiker and Gudmundsson 2004; Sultan et al. 2008). Recharge from the deep aquifers through near-surface joints and fractures could be expected, as well as recharge from the Nile aquifer in the present study. The deeper aquifer of Nubian Sandstone is potentially good for agriculture because it is recharged by water during heavy rainfall events. Along the wadis, stream captures by recent tectonics have lead to new channels along the weakness zones, e.g., fractures and fault zones which would have increased the secondary porosity and hydraulic activities as in the main Wadi Matula fault/fracture systems. The capture of represent rupture transmitter zones facilitated the recharge and discharge processes,

e.g., field observation (Fig. 11f) records that the well number 7 in El-Laqeta area lies mostly at the intersection point between the fault systems, active streams, and the paleodrainage lines (Fig. 11).

Based on the collected field data and observations, the wadi filling occurred by thick fluvial deposits of interbedded sand and gravel of probable Pleistocene age. The considerable thickness of these deposits promotes high runoff infiltration along channel beds following sporadic rain showers on the Red Sea highlands. These can be considered as prime locations for subsurface conduits for groundwater accumulation. Several water samples from two aquifers have been collected in Wadi Matula including shallow Quaternary aquifers and deep Nubian Sandstone aquifer of Cretaceous age. Highly productive wells are shown in the mapped area of the best groundwater potentials.

Conclusion

Radarasat-1 images and SRTM data interpretations revealed the development of paleodrainage courses in the study area. Radar images allowed better understanding of the history of paleochannels and their fluvial pathways. They also have produced pictorial views of the drainages and fault lines under fluvial covers here for the first time. Radarsat-1 and fused Radarsat-1/ETM+ images showed several incised gorges (E-W) that converge near the downstream area intersected by the NW gorges.

In addition to delineating the paleochannels, tectonic capture processes, and faults/fractures, the present study addressed future exploration for groundwater potentiality. This was achieved by compiling the present landscape setting with the hydrological factors that control the recharge and discharge processes and can help in predicting the best locations for groundwater potentials. These data are combined with the intersections of paleodrainage channels, stream drainage pattern, and active streams of recent flash flood.

The analysis of radar images confirmed that a probable physical continuity between present drainage system links Qena system northward and Batur system southward during the late Tertiary. Active tectonics during Pliocene/Pleistocene forced the drainage to flow westward by the breaking apart of the plateau. This seems to have occurred rapidly along the E-W and NW-SE trends related to the Red Sea tectonics that influenced the stream capture processes. This was confirmed from integrating SRTM DEM-derived stream networks, digitized paleochannels, and the active streams. The intersections between the two trends are employed in groundwater predictions. Therefore, data from paleodrainage, active streams, and fault cross-cutting relations are recommended for predicting the best sites of well locations. Moreover, sizable fluvial deposit of Pliocene/Pleistocene provided a conduit for recharging the surface runoff into the underlying aquifers.

The suggested groundwater sites were correlated with the collected well locations in Wadi Matula. The highly productive wells are confined along the intersection areas of faults, active streams, and paleodrainages. These results suggested a relationship between the discharged water wells or springs and tectonic activities. This is significant given that the modern hydrograph of the valley is defunct and the daily precipitation is only 0.0045 to 0.036 mm/day. This revealed that the discharge processes of the underlying fossil aquifers occur mostly along fault/fracture zones.

The overall results revealed that the interpretations of radar images improved the near-surface pictorial views beneath the fluvial cover and allowed understanding of the recharge and discharge processes of both the local shallow and deep regional aquifers. Detailed geophysical and field investigations are needed to verify the proposed structural features.

References

Abdalla F (2012) Mapping of groundwater prospective zones using remote sensing and GIS techniques: a case study from the Central Eastern Desert, Egypt. J Afr Earth Sci 70:8–17

Abdel Razik TM, Razvaliaev AV (1972) On the tectonic origin of the Nile Valley between Idfu and Qena, Egypt. Egypt J Geol 16:235–244

Abdelkareem M (2012) Space data and GIS applications for arid region: Wadi Qena, Egypt. PhD thesis, Faculty of Science, South Valley University, Egypt; 251

Abdelkareem M, Ghoneim E, El-Baz F, Askalany M (2012a) New insight on Paleriver development of the Nile basin of the eastern Sahara. J Afr Earth Sci 62(1):35–40

Abdelkareem M, El-Baz F, Askalany M, Akawy A, Ghoneim E (2012b) Groundwater prospect map of Egypt's Qena Valley using data fusion. Int J Images Data Fusion 3(2):169–189

Abdelsalam MG, Robinson C, El-Baz F, Stern RJ (2000) Application of orbital imaging radar for geologic studies in arid regions: the Saharan testimony. Photogramm Eng Remote Sens 66:717–726

Amarsaikhan D, Gantuya R, Battsengel V (2009) Applications of remote sensing and geographic information systems for urban land-cover changes studies. Geocarto Int 24(4):257–271

Awad WK (1981) Geophysical investigations for groundwater at some localities within wadi Qena Eastern Desert, Egypt. 1st Annual Meeting Egypt Geophysical Society, Cairo

Babiker M, Gudmundsson A (2004) The effects of dykes and faults on groundwater flow in an arid land: the Red Sea hills, Sudan. J Hydrol 297:256–273

Conoco (1987) Geological map of Egypt, scale 1:500,000. The Egyptian General Petroleum Corporation, Cairo

Das S, Behera SC, Kar A, Narendra P, Guha S (1997) Hydrogeomorphological mapping in ground water exploration using remotely sensed data—a case study in Keonjhar District, Orissa. J Indian Soc Remote Sens 25(4):145–259

El Basstawesy M, Faid A, El Gammal E (2010) The Quaternary development of tributary channels to the Nile River at Kom Ombo area, Eastern Desert of Egypt, and their implication for groundwater resources. Hydrol Process 24:1856–1865

El-Baz F (1998) Sand accumulation and groundwater in the Eastern Sahara. Episodes 21:147–151

El-Baz F, Robinson CA, Mainguet MM, Said M, Nabih M, Himida H, El-Etr HA (2001) Distribution and morphology of paleo-channels in southeastern Egypt and northwestern Sudan. Palaeoecol Afr (Klaus Heine, editor) 27:239–258

El-Ramly IM (1980) Al Kufrah Pleistocene lake—its evolution and role in present-day land reclamation. In: Salem MJ, Busrewil MT (eds) The geology of Libya, vol 2. Academic Press, London, pp 659–670

Gaber A, Koch M, Griesh MH, Sato M (2011) SAR remote sensing of buried faults: implications for groundwater exploration in the Western Desert of Egypt. Sens Imaging 12:133–151

Gani NDS, Abdelsalam MG (2006) Remote sensing analysis of the Gorge of the Nile, Ethiopia with emphasis on Dejen-Gohatsion region. J Afr Earth Sci 44:135–150

Gheith H, Sultan M (2002) Construction of a hydrologic model for estimating Wadi runoff and groundwater recharge in the Eastern Desert, Egypt. J Hydrol 263:36–55

Gudmundsson A (2001) Fluid overpressure and flow in fault zones: field measurements and models. Tectonophysics 336:183–197

Hayakawa EH, Rossetti DF, Valeriano MM (2010) Applying DEM-SRTM for reconstructing a late Quaternary paleodrainage in Amazonia. Earth Planet Sci Lett 297:262–270

Jensen JR (2000) Remote sensing of the environment: an Earth resource perspective. Prentice-Hall, Englewood Cliffs, p 544

Jenson SK, Domingue JO (1988) Extracting topographic structure from digital elevation model data for geographic information system analysis. Photogramm Eng Remote Sens 54:1593–1600

Kummerow C, Barnes W, Kozu T, Shiue J, Simpson J (1998) The tropical rainfall measuring mission (TRMM) sensor package. J Atmos Ocean Technol 15:809–817

Lopes A, Touzi R, Nezry E (1990) Adaptive speckle filters and scene heterogeneity. IEEE Trans Geosci Remote Sens 28:992–1000

McCauley JF, Breed CS, Schaber GG, Breed C, Hynes CV, Grolier J, Issawi B, Elachi C, Blom R (1982) Subsurface valleys and geoarchaeology of Egypt and Sudan revealed by Radar. Science 218:1004–1020

McCauley JF, Breed CS, Schaber GG, Mchugh WP, Issawi B, Haynes CV, Grolier MJ, El Kilani A (1986) Paleodrainages of the eastern Sahara: the Radar Rivers revisited (SIR-A/B implications for a midtertiary trans-African drainage system). IEEE Trans Geosci Remote Sens 24(4):624–648

Mertes LAK (2002) Remote sensing of riverine landscapes. Freshw Biol 47:799–816

Paillou P, Schuster M, Tooth S, Far T, Rosenqvist A, Lopez S, Malezieux J (2009) Mapping of a major paleodrainage system in eastern Libya using orbital imaging radar: the Kufrah River. Earth Planet Sci Lett 277:327–333

Paul MM, Koch M (2011) Computer processing of remotely sensed images, 4th edn. Wiley-Blackwell, Hoboken, p 434

Pohl C, van Genderen JL (1998) Multisensor image fusion in remote sensing: concepts, methods and applications. Int J Remote Sens 19:823–854

Ricchetti E (2001) Visible-infrared and radar imagery fusion for geological application: a new approach using DEM and sun-illumination model. Int J Remote Sens 22:2219–2230

Robinson CA, El-Baz F, Singhroy V (1999) Subsurface imaging by Radarsat: comparison with Landsat TM data and implications to groundwater in Selima area, Northwestern Sudan. Can J Remote Sens 25(3):268–277

Robinson CA, El-Baz F, Ozdogan M, Ledwith M, Blanco D, Oakley S, Inzana J (2000) Use of radar data to delineate paleodrainage flow direction in the Selima sand sheet, Eastern Sahara. Photogramm Eng Remote Sens 66:745–753

Roth LE, Elachi C (1975) Coherent electromagnetic losses by scattering from volume in homogenities. IEEE Trans Antennas Propag 23:674–675

Said R (1981) The geological evolution of the River Nile. Springer Verlag, New York, p 151

Sandford SK (1929) The Pliocene and Pleistocene deposits of Wadi Qena and of the Nile Valley between Luxor and Assiut (QAU). Q J Geol Soc 85:493–548

Schaber GG, McCauley JF, Breed CS (1997) The use of multifrequency and polarimetric SIR–C/X–SAR data in geologic studies of Bir Safsaf, Egypt. Remote Sens Environ 59:337–363

Schurman HM (1956) Das Parkambrin der Arabischen Waste Aegyptens. Geol Rundsch 45:179–193

Sultan M, Wagdy A, Manocha N, Sauck W, Abdel Gelil K, Youssef AF, Becker R, Milewski A, El Alfy Z, Jones C (2008) An integrated approach for identifying aquifers in transcurrent fault systems: the Najd shear system of the Arabian Nubian shield. J Hydrol 349:475–488

Thurmond AK, Abdelsalam M, Thurmond J (2006) Optical-radar-DEM remote sensing data integration for geological mapping in the Afar Depression, Ethiopia. J Afr Earth Sci 44:119–134

Zebker HP, Rosen P, Hensely S, Mouginis-Mark (1996) Analysis of active lava flow on Kilauea volcano, Hawaii, using SIR-C radar correlation measurements. Geology 24(6):495–498